1979Ap&SS..65..129K

NUCLEATION, GROWTH AND TRANSFORMATION OF AMORPHOUS AND CRYSTALLINE SOLIDS CONDENSING FROM THE GAS PHASE*

E. KRIKORIAN AND R. J. SNEED

Applied Research Laboratory, General Dynamics/Pomona Division, Pomona, Ca., U.S.A.

Abstract. The condensation of solids was investigated from the initial nucleation stage through continuous film growth, using evaporation and high-energy ion-beam sputtering. At all stages the kinetics of the nucleation process and the structural characteristics of the condensed phase (glassy, polycrystalline and monocrystalline) were defined. Although many condensates were explored, the specific system discussed is germanium condensing on a variety of amorphous and crystalline substrates.

The kinetic behavior observed in crystalline deposits was found consistent with the accepted atomistic model for nucleation. This allowed determination of such nucleation parameters as: the activation energies of surface diffusion, Q_d and adsorption, Q_{ad}, the critical nucleus size, n^*, and others. Values of such parameters were found to be systematic functions of the kinetic energy and flux of incident particles and of the type and temperature of the substrate.

Two flux and temperature dependent structural order transitions were observed in the very initial nucleation stages and found to coincide with corresponding transitions in n^*. Correlation was also established between these transitions and two structural transitions occurring during continuous film growth. This was aided by the occurrence of all four transitions in intermediate condensation stages, i.e. prior to coalescence of nucleation clusters into continuous film.

All results were very distinctly affected by the vapor state of the adsorbates, implying considerable correlation between condensation on solid surfaces and in a vapor.

1. Introduction

During early work on thin film epitaxy the authors (Krikorian and Sneed, 1966) found that growth kinetics and structural properties of films could be very systematically controlled by parameters such as substrate temperature, incident particle flux and particle energy. Further work showed that these findings applied very generally to a large number of materials and compounds. To gain further insight into the controlling mechanisms, a study was undertaken to explore the early nucleation processes as a function of the earlier observed thin film control parameters. To correlate the resulting nucleation behavior with the continuous film growth characteristics, the condensation process was traced from the formation of the very initial critical or stable nuclei through the growth into coalesced matter. At each stage of the process the objective

* Invited contribution to the Proceedings of a Workshop on *Thermodynamics and Kinetics of Dust Formation in the Space Medium*, held at the Lunar and Planetary Institute, Houston, 6–8 September, 1978.

Astrophysics and Space Science **65** (1979) 129–154. 0004-640X/79/0651-0129$03.90
Copyright © 1979 by D. Reidel Publishing Co., Dordrecht, Holland, and Boston. U.S.A.

© Kluwer Academic Publishers • Provided by the NASA Astrophysics Data System

IP Bridge Exhibit 2066
Western Digital v. IP Bridge
IPR2024-01447

1979Ap&SS..65..129K

was the definition of: (a) the substrate and gas phase parameters governing the kinetics of the process, (b) the conditions leading to the formation of either glassy (amorphous) or crystalline solid phases, and (c) the conditions causing the transition of the condensed phase from an amorphous to a crystalline state. Results of this work constitute the content of this paper.

The relevancy of this work to the study of condensation phenomena in a space environment is not based on the specific materials experimentally explored, but on the phenomenological behavior patterns and the methodology for analyzing the experimental observations. That is, the information and methodology can be directly applied to the study or analysis of condensation on solid surfaces exposed to a flux of atomic and molecular particles in any low pressure environment and indirectly to the analysis of condensation phenomena occurring in the gaseous cloud prior to or without condensation on a solid surface.

2. Experimental

A diversified and extensive range of experimental parameters and conditions were explored. These included: particle flux density, particle energies, particle type, background pressures, substrate temperature, substrate type and substrate surface conditions. Obviously, all of these parameters correspond to parameters describing conditions that may be encountered in a space environment. However, the range of parameter values occurring in space may be different from those investigated here. The following summarizes these ranges. The gas phase particle flux densities were controlled from as low as that required to form an atomic layer per minute ($\sim 10^{14}$ cm^{-2} sec^{-1}) to as high as required for a condensation rate of about 1000 layers per minute ($\sim 10^{17}$ cm^{-2} sec^{-1}). The kinetic energy of the gase phase particles was controlled to achieve values ranging from thermal levels (ambient) to values of several hundred electron volts. Experiments covering all stages of condensation, i.e. from very initial nucleation through continuous layers were mainly performed with two monatomic substances – germanium and tantalum, with germanium the most thoroughly studied. In experiments on post-nucleation growth kinetics and structural transitions a considerably larger variety of materials was used, including: dielectric, semiconductor and metallic substances as well as monatomic and compound particles. The latter included compounds reactively formed on the substrate surface from a monatomic beam in the presence of a partial pressure of reactive gas. The environmental backgrounds ranged from high to ultra-high vacuum conditions. Most data were generated in the 10^{-8} torr range. Condensation studies inside an electron microscope were carried out at pressures in the high 10^{-7} torr range. Reactive depositions occurred in partial pressures in the range of 10^{-6} to 10^{-5} torr. Substrate temperatures were controlled from ambient temperature to over 1000 K. The substrates used had structures ranging from amorphous or glassy to polycrystalline and monocrystalline. Also selected were materials with different hardnesses and different thermal conductivities. Specific

© Kluwer Academic Publishers • Provided by the NASA Astrophysics Data System

1979Ap&SS..65..129K

substrate materials included carbon, graphite, germanium, mica, CaF_2 and others. Different substrate surface conditions were achieved by using cleaved and polished substrates and surfaces with impurity imperfections induced by background pressure variations. The work reported here will address only a number of selected substrate types to demonstrate the effects.

The experimental techniques used to generate the gas phase to be condensed were vacuum evaporation and ion-beam sputtering, the former yielding the low kinetic energy particle flux while the latter generated the high energy flux. Specifically, ion-beams having energies ranging from 1 kV to 30 kV were used.

Many of the evaporation experiments were carried out in an electron microscope for *in situ* observations of the processes. This was, of course, most desirable. However, since only relatively low formation rates can be observed in this manner, higher rates were explored in an UHV station, but not until full correlation between low rate results was achieved by both techniques.

The ion-beam sputtering system was ideal for this work since it operates with an ultra-high vacuum environment during sputtering (10^{-7} torr) and does not entail the plasma 'interaction' with the sputtered particles typical for other sputtering techniques. Also, in an ion-beam system, the beam energy can be directly controlled by an acceleration potential, i.e. it is not dependent on the plasma conditions as is typical for other sputtering techniques.

The vapor generated by both evaporation and sputtering was essentially neutral.

Electron microscopy was almost exclusively used as the analytical tool. Where substrates permitted, transmission electron diffraction was used to determine the structural characteristics of the deposits, while reflection diffraction was used when no transparent substrates were involved. Determination of size, shape and density characteristics of nucleation clusters as a function of time and deposition conditions was carried out by two methods – either by direct transmission electron microscopy when thin substrates were involved or by electron microscopy of 'stripped' deposits embedded in either a carbon or a silicon monoxide film. By both techniques, nucleation clusters as small as 15 to 20 Å in diameter were detectable and measurable. Actual measurements were performed on micrographs, enlarged up to 400 000 × – depending on cluster size and density.

3. General Film Formation History

As indicated in the introduction, the work reported here was initiated on the basis of some interesting observations made during studies on the epitaxy of thin films. Figure 1 illustrates these observations schematically. A so-called structural phase diagram which applies to virtually all material systems investigated is shown. Depending on substrate temperatures and deposition rates, films are formed having either amorphous, polycrystalline or single crystalline structures. The polycrystal to single crystal transition, defined as expitaxial transition, is obviously very temperature and rate dependent. It

© Kluwer Academic Publishers • Provided by the NASA Astrophysics Data System

1979Ap&SS..65..129K

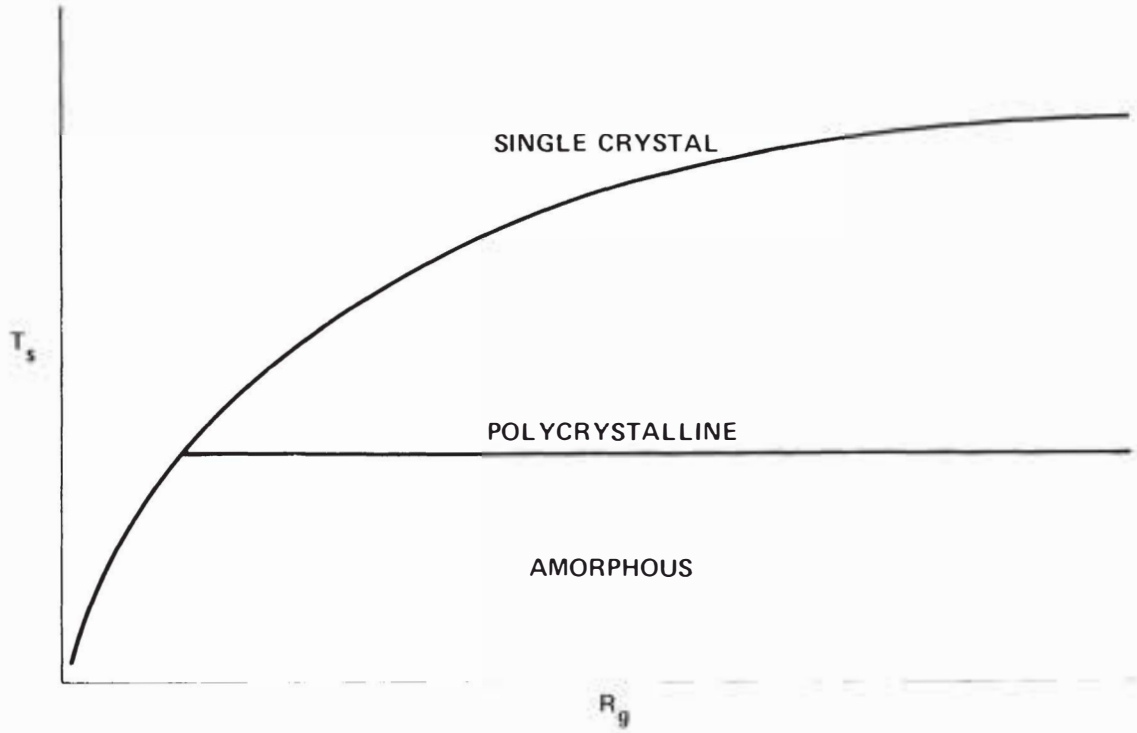

Fig. 1. Film structure diagram.

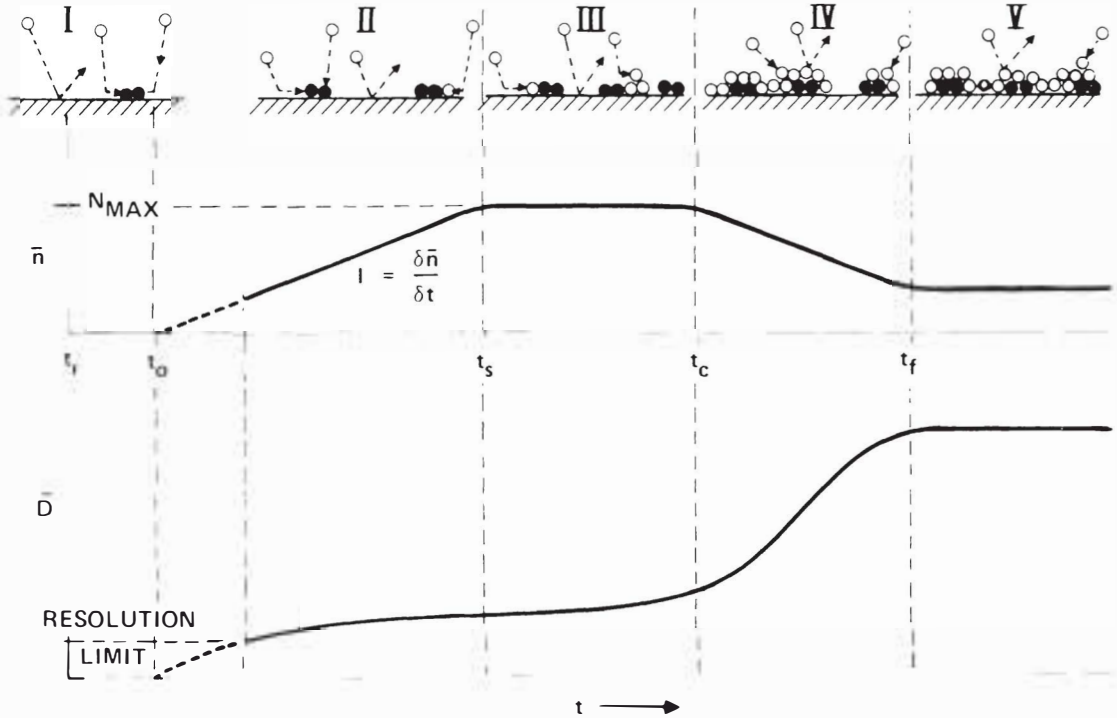

Fig. 2. Film formation history.

© Kluwer Academic Publishers • Provided by the NASA Astrophysics Data System

1979Ap&SS..65..129K

was possible to describe this transition quantitatively as a function of particle surface diffusion and condensation rates as well as of the particle and substrate material parameters. By contrast, the transition from the amorphous to the crystalline state was found to be only temperature dependent. It required the nucleation studies reported here to reveal the mechanisms controlling this transition.

Figure 2 shows schematically the total film formation history, in terms of the average nucleation density ($\bar{n}$) and average cluster diameter $\bar{D}$ as a function of time. Five stages are shown: Stage I, the induction time; Stage II, the initial nucleation stage (both cluster density and size increase with time, virtually unaffected by neighboring clusters); Stage III, the saturation stage (cluster density has reached the maximum value (N_{max}) that can be accommodated by a given substrate at a given condition; therefore, $\bar{n}$ remains constant with time but the clusters continue to grow in size due to growth of adatoms to the clusters); Stage IV, the coalescence stage (cluster density decreases rapidly, due to cluster coalescence) and, finally, Stage V, the continuous film growth stage. In the following sections some actual experimental results obtained during the various stages of nucleation are presented.

4. The Nucleation Kinetics – Typical Experimental Results and General Observations

Figure 3 shows observed temperature and particle flux effects on the generation of nucleation clusters $\bar{n}$, on the saturation density N_{max}, and on the rate of nucleation $I = dn/dt$ during the condensation of Ge on a graphite substrate. As a measure of particle flux, the measured growth rate is used for convenience. For a given condition and material system, the growth rate is directly proportional to the particle flux. The negative slopes in Figure 3 correspond to coalescence of clusters as time proceeds. As can be seen, I, N_{max} and $\bar{n}$ increase with decreasing temperature and increasing growth rate. As shall be seen, this is one factor which establishes the consistency of the nucleation behavior with accepted general theories on nucleation and condensation.

Figure 4 shows similar data comparing the results of depositions by sputtering and evaporation, this time on a CaF_2 substrate. The dependence of $\bar{n}$, I and N_{max} on substrate temperature has obviously the same trend as that observed on the graphite substrate. The comparison between the evaporation and ion-beam sputtering results in Figure 4 reveals that N_{max} is lower for sputtered than for evaporated deposits – at equivalent temperatures. This is a kinetic energy effect which will be discussed below.

A typical effect of the substrate material is illustrated in Figure 5. The two substrates used for these experiments were carbon and graphite, i.e. representative of amorphous and crystalline materials with similar properties. It is apparent from the data in this figure that for both sputtering and evaporation $\bar{n}$, $d\bar{n}/dt$ and N_{max} are all higher on the carbon substrate than on the graphite substrate. It should be noted that the substrate temperature and deposition rates are of the same magnitude in both cases. The observed substrate effects are due to the fact that an amorphous substrate can contain

© Kluwer Academic Publishers • Provided by the NASA Astrophysics Data System

1979Ap&SS..65..129K

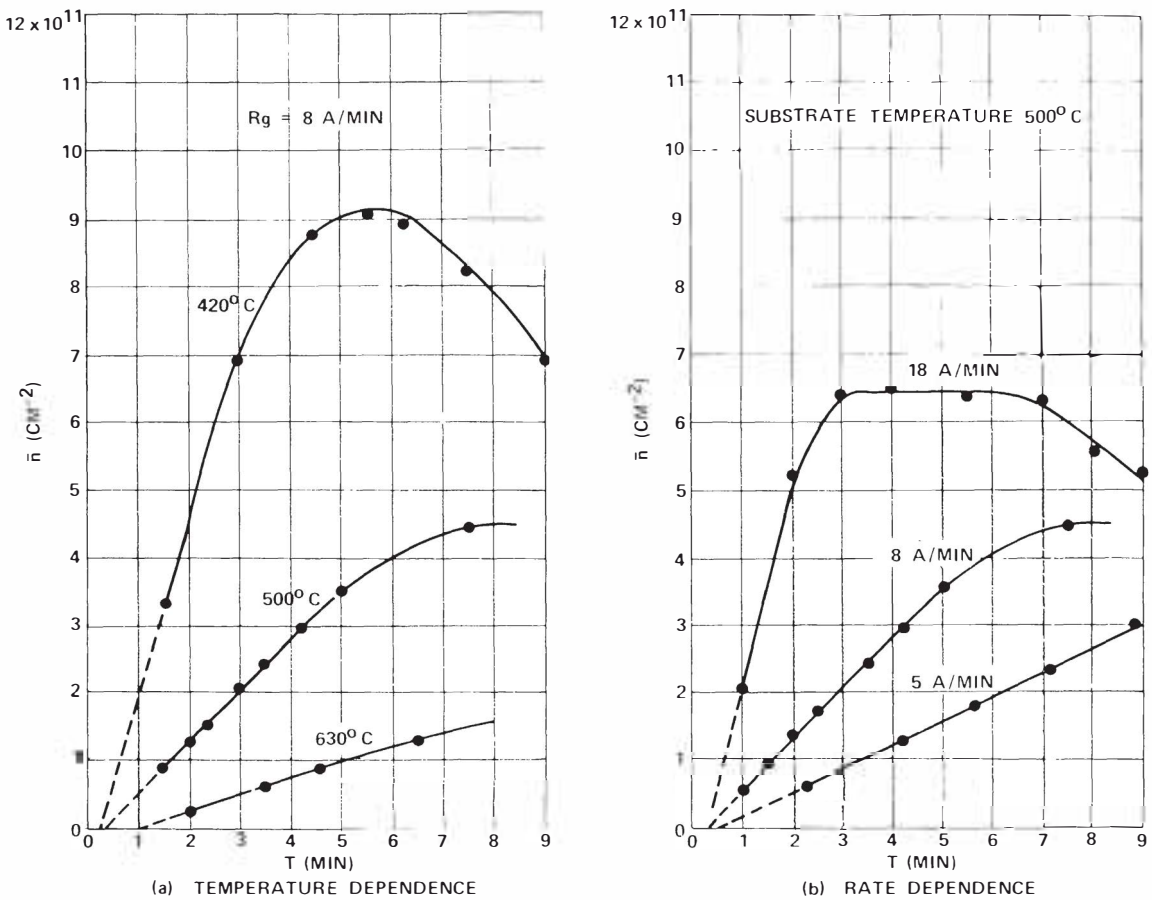

Fig. 3. Nucleation history – germanium on graphite by *in situ* evaporation.

more potential nucleation (or low energy) sites than a crystalline substrate. It should be noted that N_{max}, $\bar{n}$ and $d\bar{n}/dt$ are higher for ion-beam sputtering than evaporation for both substrates. This is opposite to the behavior observed on the CaF_2 substrate in Figure 4. This is again a kinetic energy effect related to the 'hardness' of the substrate.

To aid in the explanation of the various possible kinetic energy effects, Figure 6 shows a schematic illustration of three potential effects.

The first effect is a partial embedding of the incident particle which obviously increases with particle kinetic energy. Similarly apparent is that for atoms of equal kinetic energy, the penetration is a function of the substrate 'hardness'. The result of embedding is a longer mean time of stay of the individual adatom at the initial adsorption site. That is, the energy of desorption, Q_{DES}, which is proportional to the energy of adsorption, increases with penetration. This in turn will increase the probability of generating a stable nucleus and thus, in effect, an increased number of nucleation sites. This mechanism is compatible with the observation that the nucleation density and rate increases due to kinetic energy is greater on carbon and graphite than on CaF_2 and greater on carbon than on graphite.

The second effect described is that of surface mobility ($\mu \sim \exp - (Q_d/RT)$ which

© Kluwer Academic Publishers • Provided by the NASA Astrophysics Data System

1979Ap&SS..65..129K

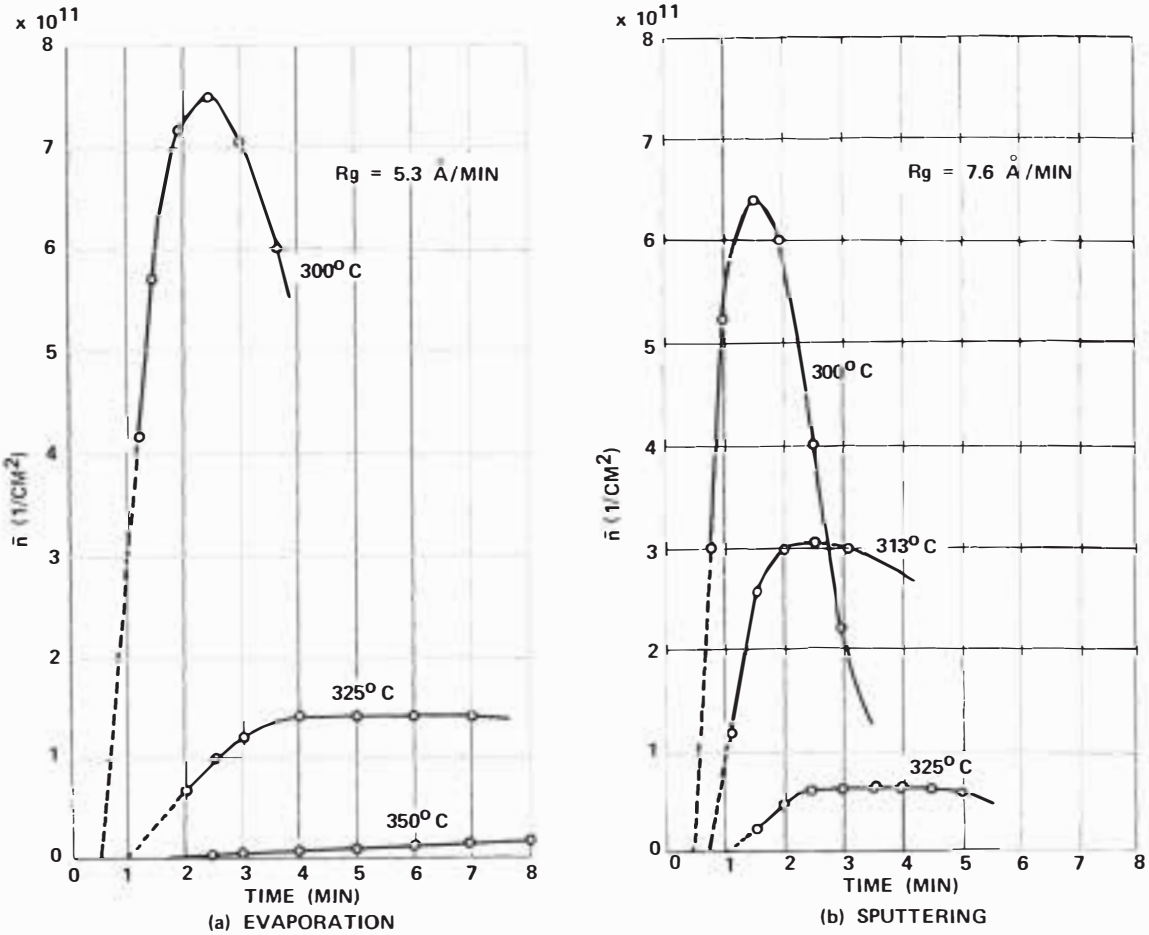

Fig. 4. Temperature dependence of nucleation rate (Ge on CaF_2 by UHV evaporation and IB sputtering).

controls the mean time of stay, the probability of the adatom finding the lowest energy nucleation site and/or the probability of collision with other adatoms to form a critically sized nucleus during its mean time of stay. Important for the observations given later, is that the mobility also controls the ordering process of the adatoms or critical nuclei and therefore the probability of forming a crystalline structure. In low energy condensation the surface temperature imparts the energy for the surface mobility. For high energy incidence the particle may retain part of the energy, the magnitude being controlled by the momentum loss on collision, the heat dissipation from the substrate surface (i.e., k_T) and the degree of embedding which, in effect, controls the energy for surface diffusion, Q_d, of the adsorbate. Another model, leading to the same results, is that the non-dissipated impact energy raises the temperature of the very surface and therefore the surface mobility. Many of these are competing mechanism. However, three factors are usually predominant. First, the mobility will be higher for equal particle energy and substrate temperature, on substrates with lower k_T. Secondly, the mobility for identical conditions will be higher on harder materials. Thirdly, the lowest energy for nucleation (or physical adsorption) is normally found at already condensed nuclei or nucleation clusters rather than on the

© Kluwer Academic Publishers • Provided by the NASA Astrophysics Data System

1979Ap&SS..65..129K

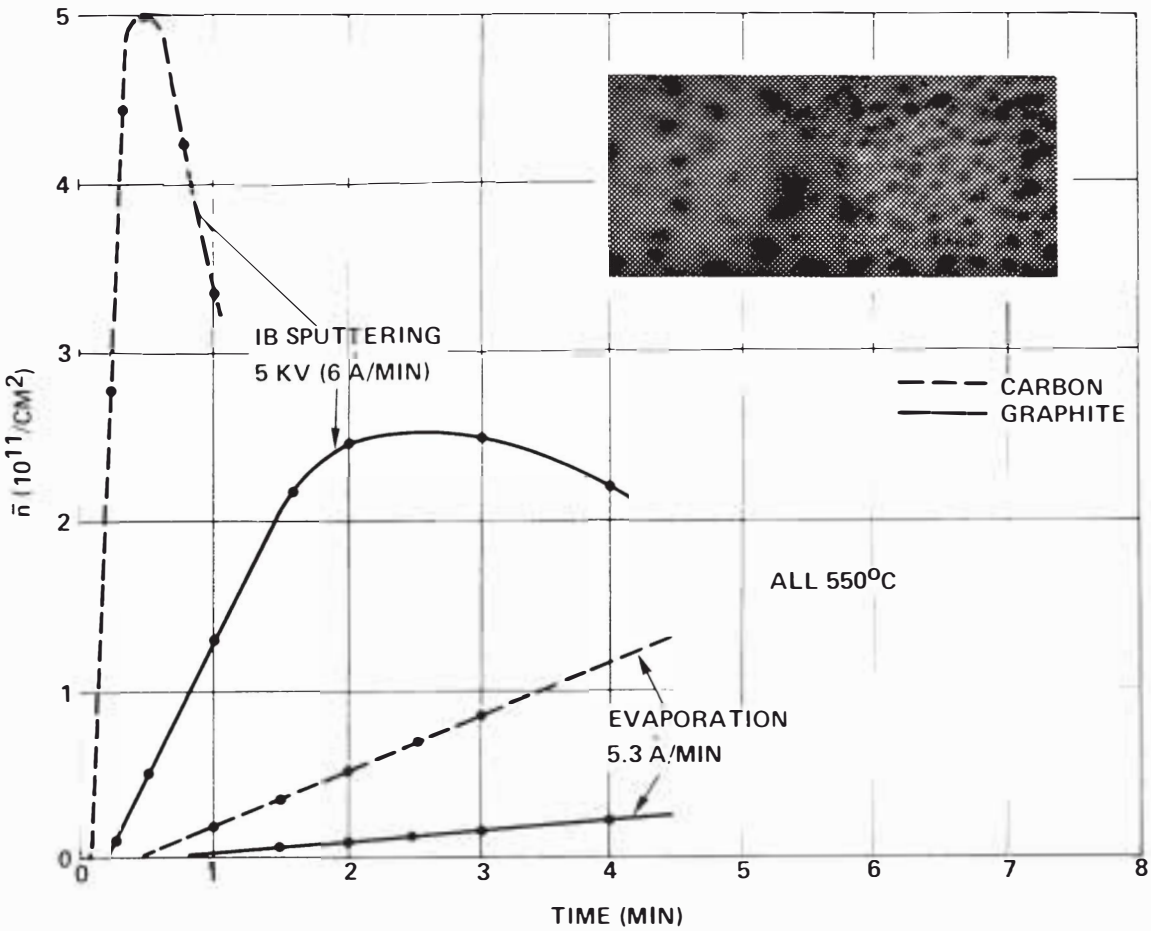

Fig. 5. Substrate dependence of nucleation rate (Ge on carbon and graphite).

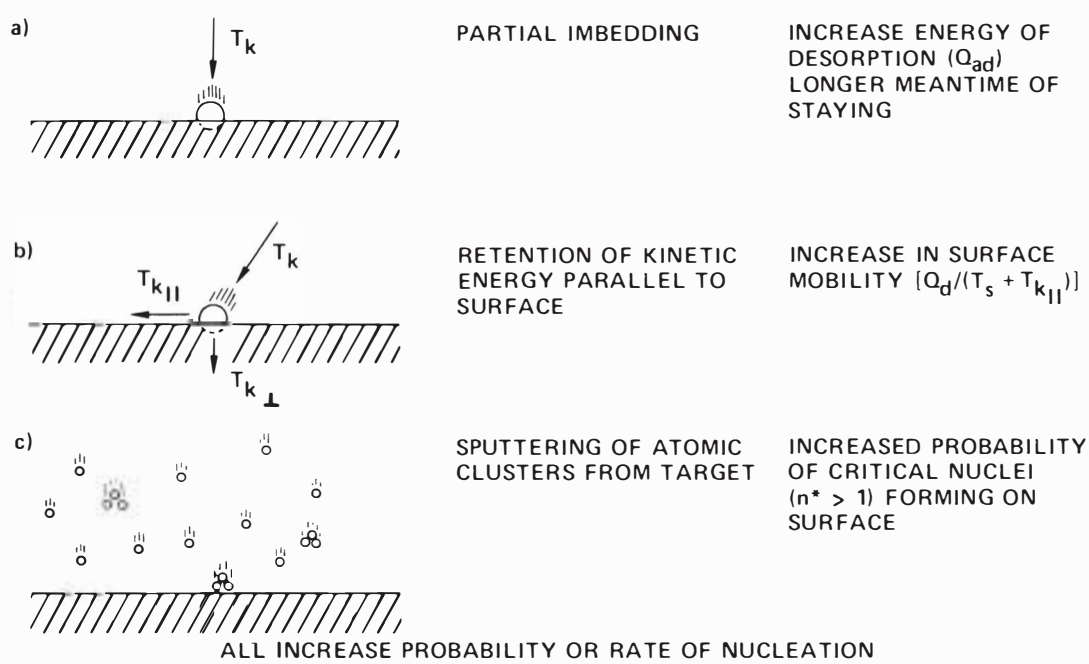

Fig. 6. Effects of particle kinetic energy.

© Kluwer Academic Publishers • Provided by the NASA Astrophysics Data System

1979Ap&SS..65..129K

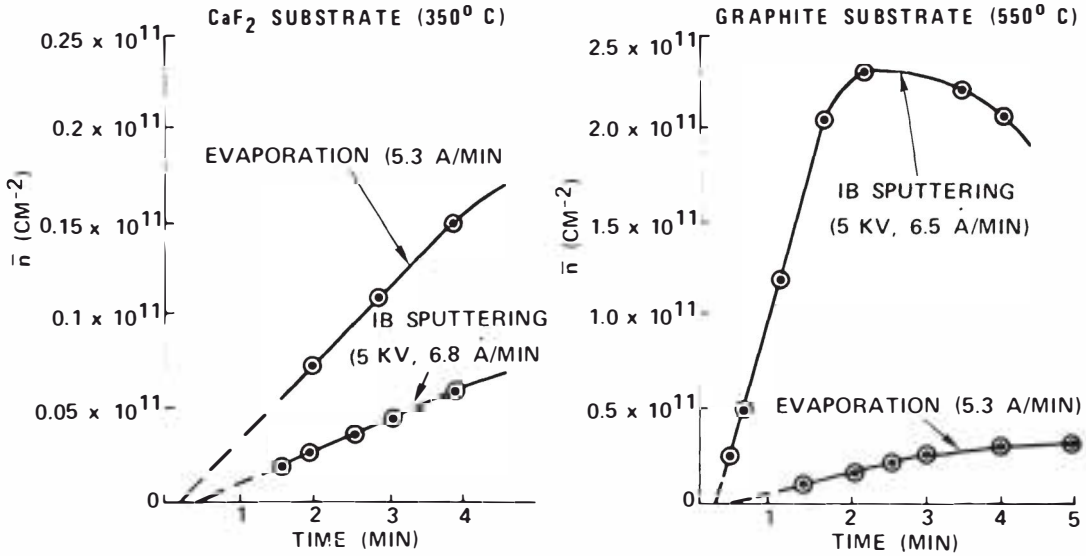

Fig. 7. Nucleation history – UHV evaporation vs. UHV ion beam sputtering.

strange substrate. These are the apparent reasons that for equal energies, the density and rate of formation of nucleation sites is lower, and the maximum cluster size larger, on CaF_2 than on carbon and graphite. CaF_2 is the poorer thermal conductor and the harder material.

The third effect, influencing some results discussed later, is critical when the incident beam contains multiatomic particles; this increases the probability of stable nuclei (when the critical nucleus size $n^* > 1$) directly adsorbing on the surface – and consequently increases the nucleation rate and density. Likewise, Q_{ad} and Q_d, of a given adsorbate will increase, thus reducing the mobility. This effect has impact on condensation of diatomic or molecular vapors. In our study it was also important in the evaluation of experimental results, since the probability of generating multiatomic beam components increases with sputtering energy.

For a more direct illustration of the first two effects, and the relative predominance of each, data such as shown in Figure 7 can be used. Evaporation and IB sputtering results are compared side by side for CaF_2 and graphite substrates. These are representative of hard and soft surfaces and low and high thermal conductivity substrates. As discussed, higher kinetic particle energy will: (a) increase N_{max}, $\bar{n}$ and I if the embedding effect dominates, and (b) decrease N_{max}, $\bar{n}$ and I if residual kinetic energy effects predominate. As would be expected, on graphite, the nucleation kinetics is controlled by embedding, consistent with the softness of the substrate, and on CaF_2 by the residual kinetic energy effect, consistent with hardness and low k_T. As would also be expected, a more quantitative analysis suggests that more than one mechanism is involved simultaneously.

To demonstrate the effect of another control parameter mentioned earlier, results were compared for evaporation in different background pressure environments. An example is shown in Figure 8, by using comparable data obtained in the UHV

© Kluwer Academic Publishers • Provided by the NASA Astrophysics Data System

1979Ap&SS..65..129K

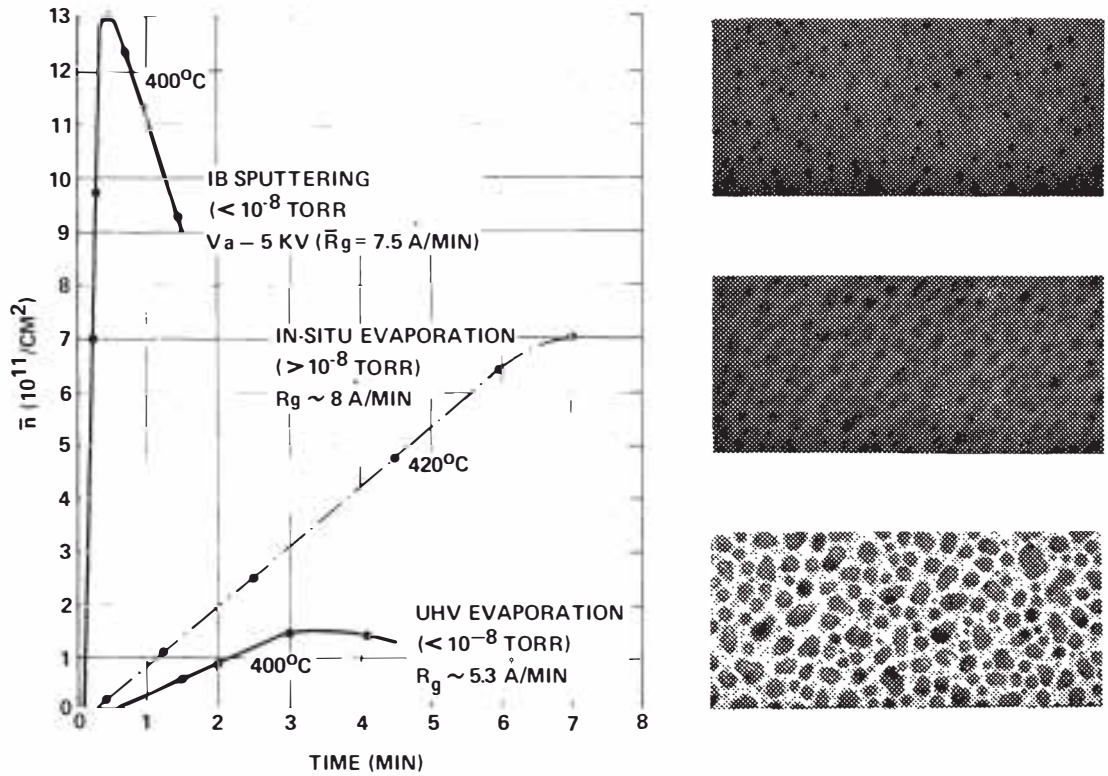

Fig. 8. Nucleation rate – evaporation vs. IB sputtering (Ge on carbon and graphite).

deposition station (10^{-8} torr range) and during evaporation in an electron microscope (modified for pressure in the 5×10^{-6} to 1×10^{-7} torr range).

The primary effect of the background pressure is the adsorption of background vapor particles which, in turn, produce potential nucleation sites by locally affecting the surface energy (or pending vapor composition by the affinity of the background adsorbates with those from the incident particle beam). The result is that $\bar{n}$, $d\bar{n}/dt$ or (I), and N_{max} will increase with higher background pressure. The magnitude of the effect will, of course, depend on the composition of the background vapor and its condensation and integration properties with both the surface and the beam particles. Obviously, the data in Figure 8 are compatible with this model.

5. Analysis of Nucleation Results and Discussion

The results presented above illustrated various effects, controlled by the conditions under which condensation takes place. In this section, these results are used, along with existing nucleation theories, to determine the more basic and general mechanisms of the nucleation and condensation process. Of interest are the parameters which control the probability of forming critical or stable nuclei, and thus the rate of nucleation. These include:

R_i, particle incidence rate;
n^*, number of atoms in a critical nucleus;
T_K, kinetic energy of incident particle;

© Kluwer Academic Publishers • Provided by the NASA Astrophysics Data System

1979Ap&SS..65..129K

T_s, substrate temperature;
Q_{ad}, activation energy of adsorption (desorption);
Q_d, activation energy of surface diffusion;
E_{n^*}, binding energy of atoms in a critical nucleus ($n^* = 1$, $E_{n^*} = 0$);
a_0, n_0, lattice constant (or diffusion path) and number of probable sites, respectively.

As stated, the initial condensation process can be quite well described by basic nucleation theories, modified for such factors as particle kinetic energy, as long as the conditions result in crystalline nucleation. For these cases, the data yielded well-defined critical nuclei sizes ($n^* + 1$) for each material system as well as expected energies of adsorption, surface diffusion, etc.

Figures 9 and 10 illustrate how the nucleation theores are utilized to analyze our experimental results. Figure 9 illustrates how plots of log I vs. I/T and log R determine values of $(n^* + 1)Q_{ad} + E_{n^*} - Q_d$ and $n^* + 1$, utilizing basic nucleation theory. Similar plots for log N_{max} vs. $1/T$ and log R_i (Figure 10) yield values of $n^*Q_{ad} + E^*$ (or Q_{ad} directly) as well as n^* (>1). From the combined results in Figures 9 and 10 the values of Q_{ad}, Q_d, E_{n^*} and n^* can then be separately defined.

With a well controlled set of experiments, the definition of these values is quite unambiguous. This is illustrated with actually measured data in Figure 11, which shows the temperature dependence of I ($= d\bar{n}/dt$) of Ge on CaF_2. Three different slopes – defining regions of different critical nucleus sizes are noted, each corresponding to a different structural region; i.e. regions in which single crystal (C_{PO}), polycrystalline (C_{RO}), and both amorphous (or glassy) and crystalline ($A + C_{RO}$) deposits occur.

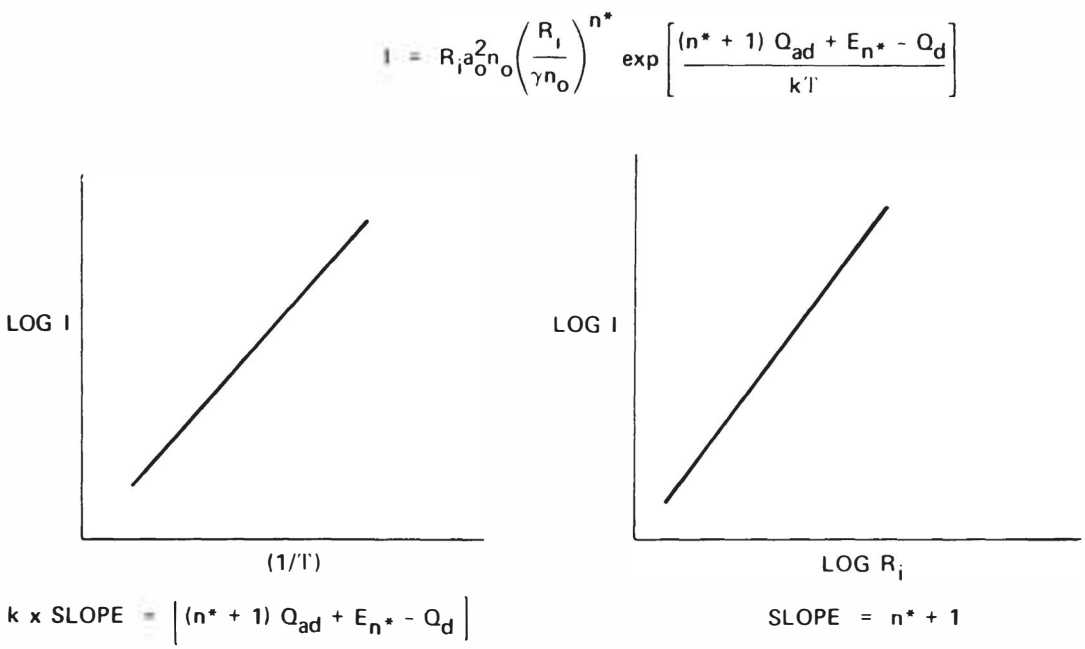

Fig. 9. Analysis of nucleation rate data.

© Kluwer Academic Publishers • Provided by the NASA Astrophysics Data System

1979Ap&SS..65..129K

$$N_{MAX} = \frac{1}{a_o}\left(\frac{R_i a_o^2}{\gamma}\right)^{n^*} \exp\left[\frac{n^* Q_{ad} + E_{n^*}}{kT}\right] \quad ; \quad (n^* > 1)$$

$$N_{MAX} = C(R_i)^{1/2} \exp\left[\frac{Q_d}{kT'}\right] \quad ; \quad (n^* = 1)$$

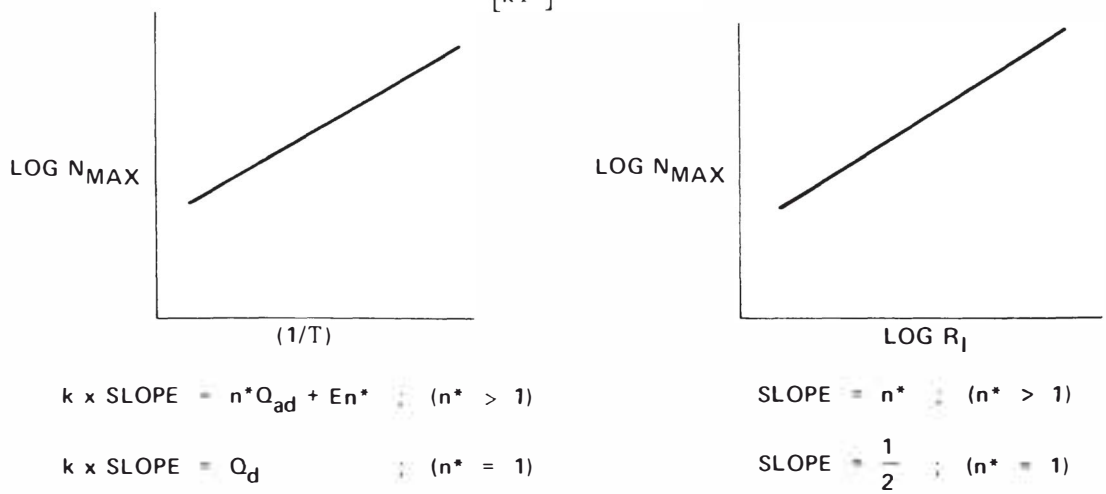

Fig. 10. Analysis of N_{max} data.

A very interesting and important result of this investigation is the observation of the region (A + C_{RO}) which we designate the recrystallization region. Nucleation and growth in this region starts with purely amorphous condensation and changes into a crystalline deposit with time. This does not conform to basic nucleation theories. Thus the behavior in this region had to first be empirically described. In this case the con-

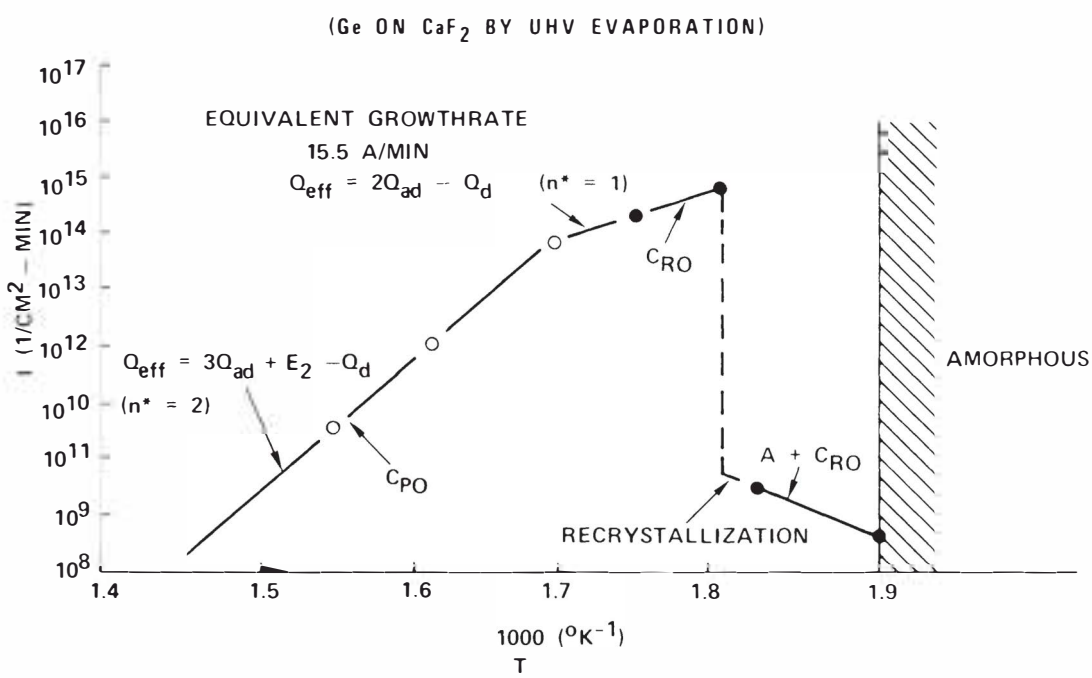

Fig. 11. Nucleation rate dependence on temperature (Ge on CaF_2 by UHV evaporation).

© Kluwer Academic Publishers • Provided by the NASA Astrophysics Data System

1979Ap&SS..65..129K

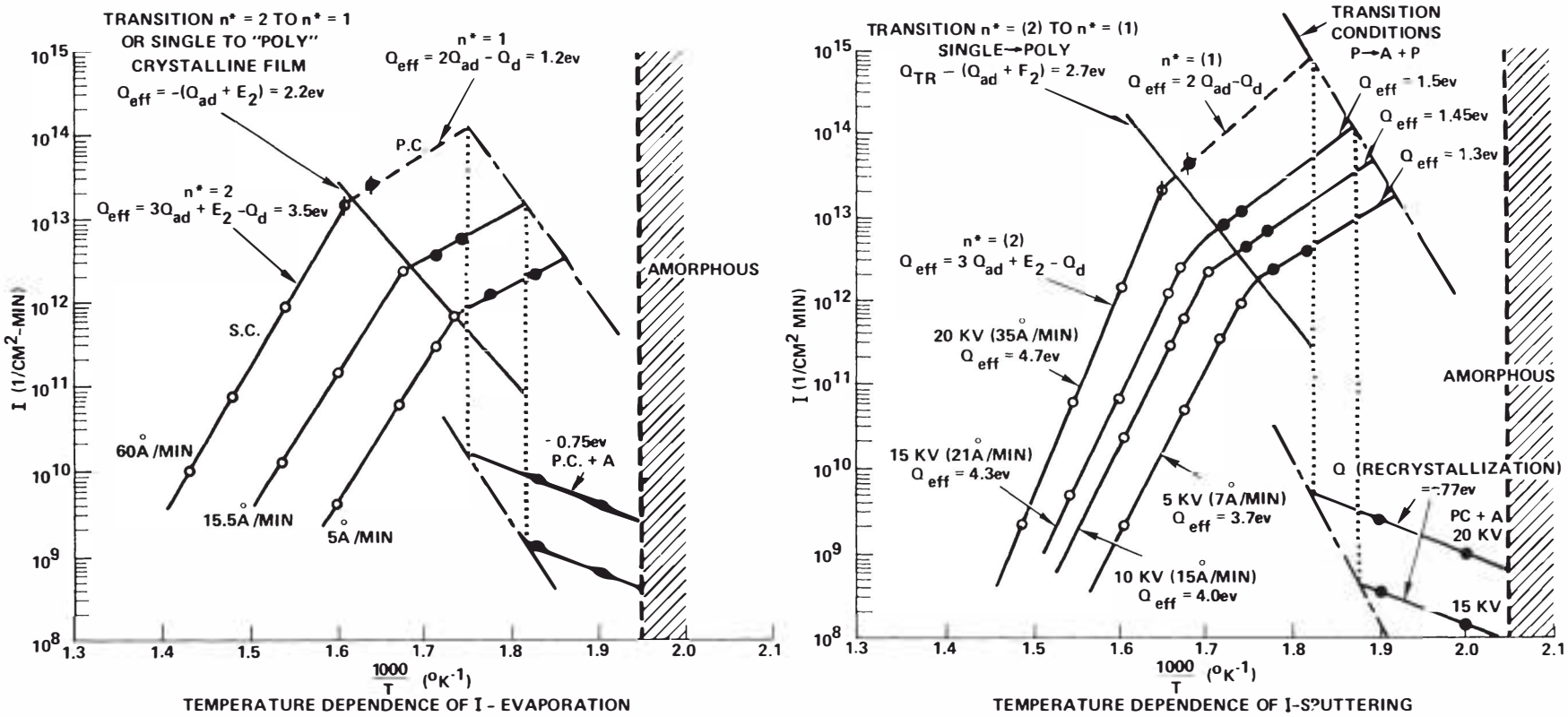

Fig. 12. Temperature dependence of nucleation rates (evaporation and sputtering).

© Kluwer Academic Publishers • Provided by the NASA Astrophysics Data System

1979Ap&SS..65..129K

densation clearly occurs at substrate temperatures and particle flux densities insufficient to support the formation of critically sized or stable nuclei. As indicated in Figure 11, the growth kinetics of the initial glassy condensate differ drastically from that of initially crystalline condensates. The effective activation energy, Q_{eff}, changes to negative values, and absolute values of I (and $\bar{n}$) differ significantly from those of purely crystalline nucleation (region C_{PO} and C_{RO}). As will be shown later, the condensation mechanism in this region is controlled by a process analogous to recrystallization, i.e. crystallites are formed from the condensate already deposited on the surface, rather than by ordering of incident particles. The temperature region in which this occurs corresponds to the amorphous to polycrystalline transition illustrated in Figure 1.

At very low temperatures, $1000/T > 1.9$ in Figure 11, the initial condensation and subsequent growth has exclusively glassy or amorphous characteristics. Here, the concept of nucleation is no longer applicable and growth occurs by simple adsorption of, typically, individual incident particles – controlled only by the 'sticking' coefficient or Q_{ad}.

The behavior illustrated in Figure 11 was found to be very consistent. As an example, Figure 12 shows comparable data for evaporation and sputtering of Ge on CaF_2 using different fluxes and particle energies. Figure 12(a) shows that for three different rates

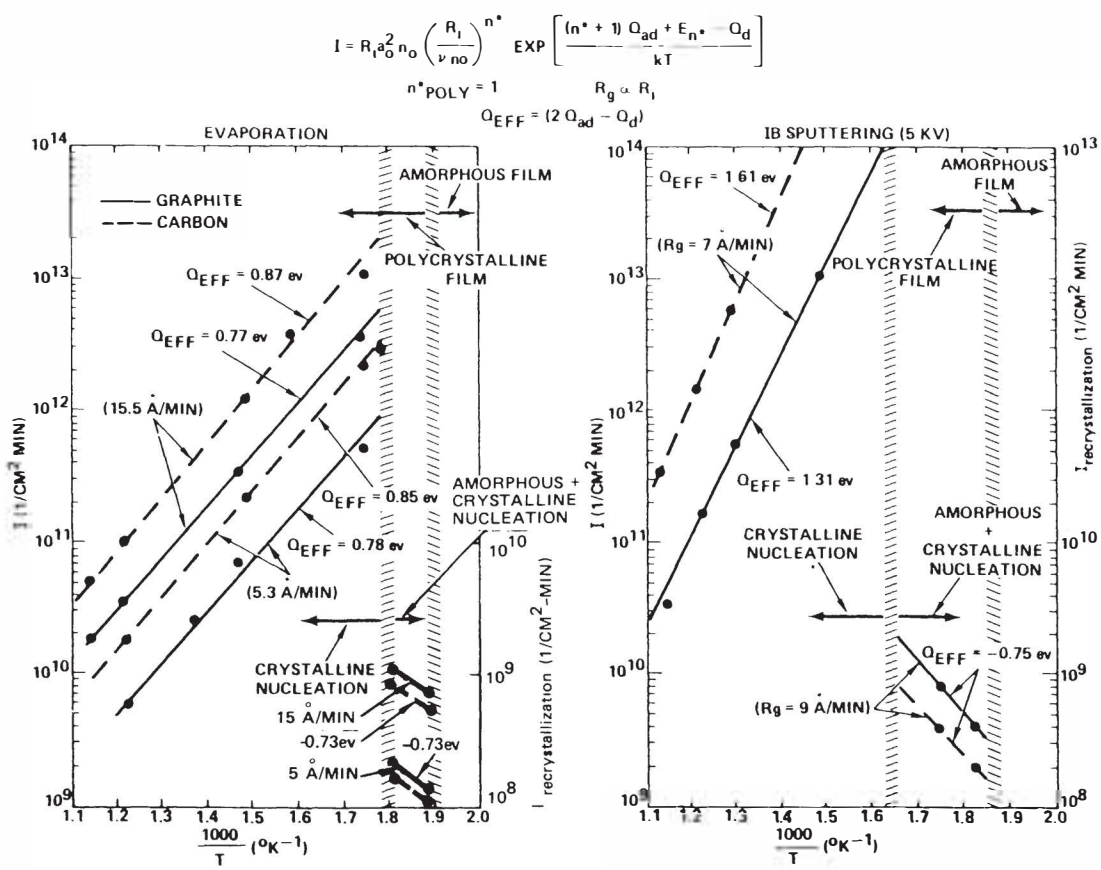

Fig. 13. Substrate dependence of nucleation rate vs. $(1/T)$ (Ge on carbon and/or graphite).

© Kluwer Academic Publishers • Provided by the NASA Astrophysics Data System

1979Ap&SS..65..129K

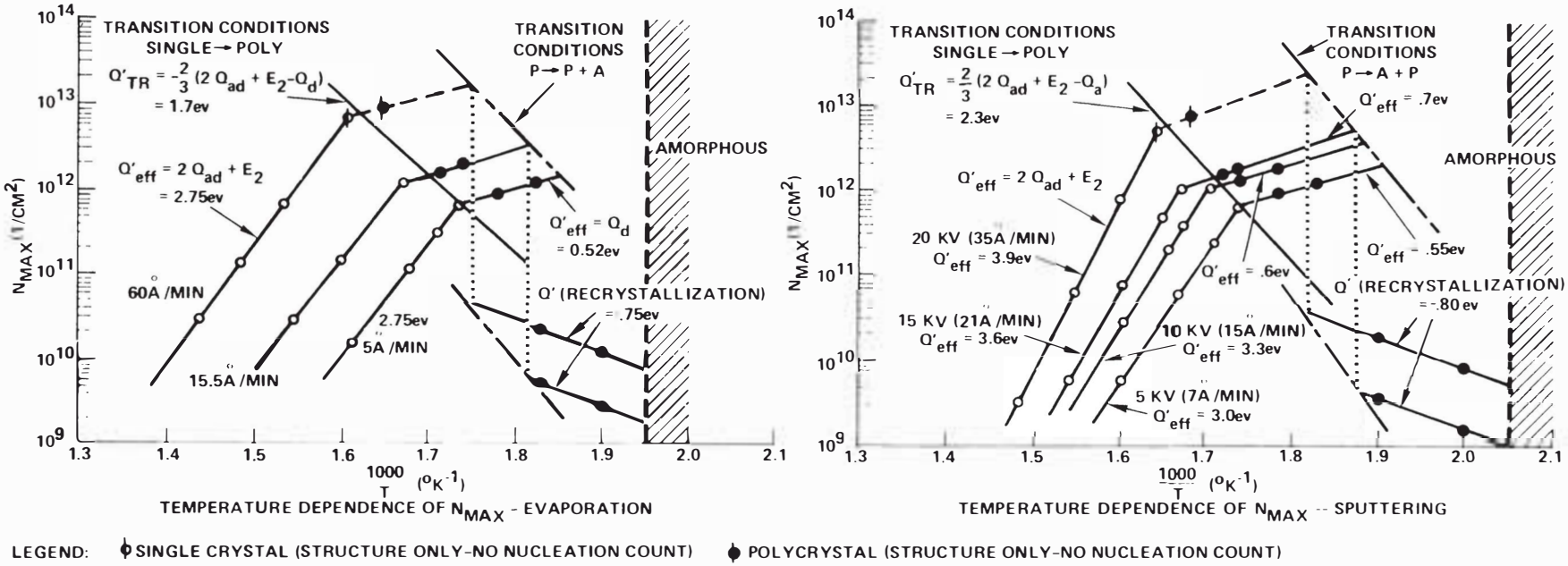

Fig. 14. Temperature dependence of the nucleation saturation density (evaporation and sputtering) – germanium on CaF_2.

© Kluwer Academic Publishers • Provided by the NASA Astrophysics Data System

1979Ap&SS..65..129K

of evaporative deposition, the slopes or effective activation energies remain constant. In Figure 12(b) we note the kinetic energy effect on the effective activation energy except in the region of recrystallization where the slopes are not affected.

Referring to the basic nucleation relation in Figures 9 and 10, the effects of the particle energy is introduced, in the crystalline nucleation range, by a $Q_{\mathrm{ad\,(effective)}}$ term (embedding effects) and an $T_{\mathrm{s\,(effective)}}$ term (residual energy affect) in the appropriate equations. In the recrystallization region, the process is controlled only by the simple diffusion equation ($\exp - Q_{\mathrm{d}}/kT_{\mathrm{s}}$) and is, therefore, independent of particle kinetic energy, if our model is correct. The results in Figure 12 are obviously supportive.

Similar results for carbon and graphite substrates, in Figure 13, indicate larger differences in activation energies between results from ion-beam sputtering and evaporation. This reveals the strong effect of embedding on $Q_{\mathrm{ad\,(effective)}}$ in these materials. Again, in the recrystallization region, the activation energies remain constant for evaporation and sputtering as expected. Furthermore, comparing the activation energies in the recrystallization region in all four sets of data in Figures 12 and 13, the effective activation energies are essentially the same – adding further proof to the model that the observed transition is controlled by the recrystallization of the con-

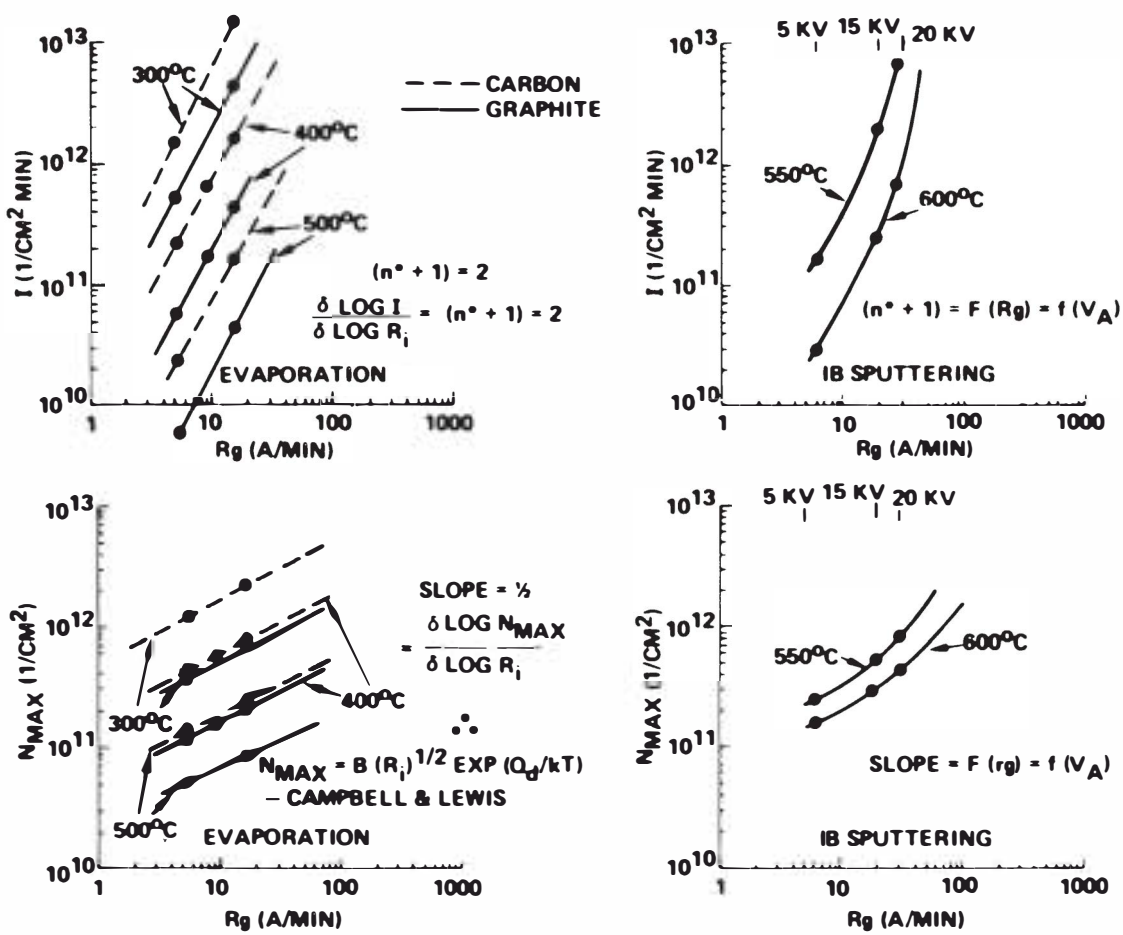

Fig. 15. Deposition rate dependence of nucleation rate and $N_{\max}$ (Ge on carbon and/or graphite).

© Kluwer Academic Publishers • Provided by the NASA Astrophysics Data System

1979Ap&SS..65..129K

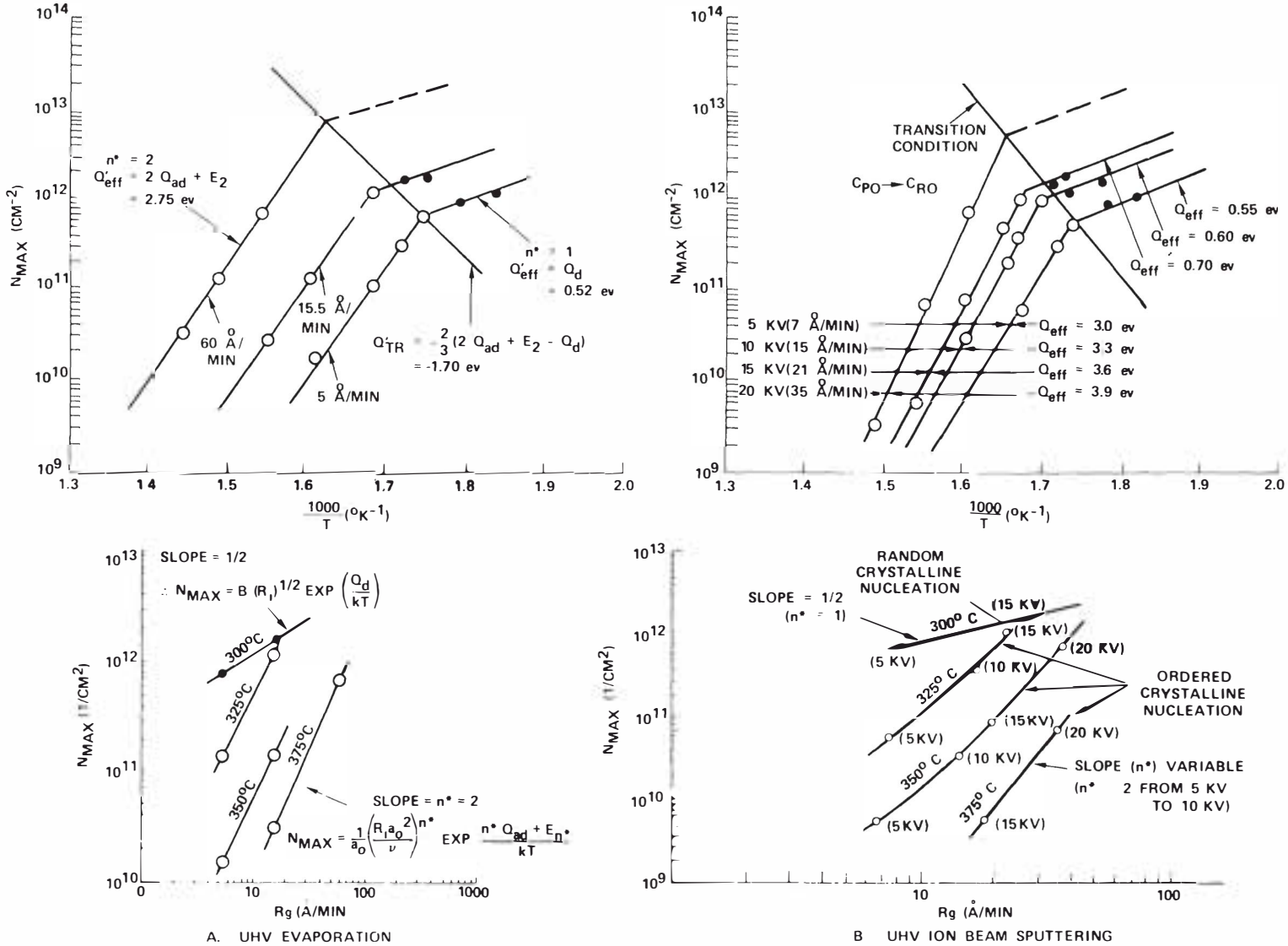

Fig. 16. Temperature and rate dependency of saturation densities – UHV evaporation vs. ion beam sputtering – Ge on CaF_2(111).

© Kluwer Academic Publishers • Provided by the NASA Astrophysics Data System

1979Ap&SS..65..129K

densed matter – which is the same in all four cases, and not by the substrate or other factors. In accordance with the relations shown in Figure 10, evaluation of the nucleation rate, I, and the maximum nucleation density, $\overline{N}_{max}$, should lead to a final definition of the parameters of interest. Examples of such analyses are shown in Figure 14 (N_{max} vs. $1/T$), Figure 15 (I and N_{max} vs. Rg) and in Figure 16 (N_{max} vs. I/T and Rg) for different substrates and kinetic energies. The figures are annotated with the respective effective activation energies, Q, as well as the parameters contributing to Q. These figures contain also a value for the activation energies for the structural transitions, Q_{TR}. These will be discussed in the next section. Without discussing all details, the results of this analysis are very unambiguous if kinetic energy effects are properly taken into account in the analysis. For all cases illustrated, these results may be summarized as follows:

(1) Independent of substrate material, flux and kinetic energy, the size of the Ge critical nucleus, $n^* = 2$ for single crystal condensation and $n^* = 1$ for polycrystalline condensation.
(2) Independent of particle flux and kinetic energy, the activation energy, for diffusion of the particle on the substrate surface $Q_d = 0.52$ eV on CaF_2 and $Q_d = 0.32$ eV on graphite and $Q_d = 0.35$ eV on carbon; also from the recrystallization data Q_d for Ge on Ge (in the amorphous state) $\simeq 0.75$ eV.
(3) Independent of particle flux and kinetic energy, the energy of adsorption (or desorption), $Q_{ad} = 0.86$ eV on CaF_2, $Q_{ad} = 0.55$ eV on graphite and $Q_{ad} = 0.60$ eV on carbon.

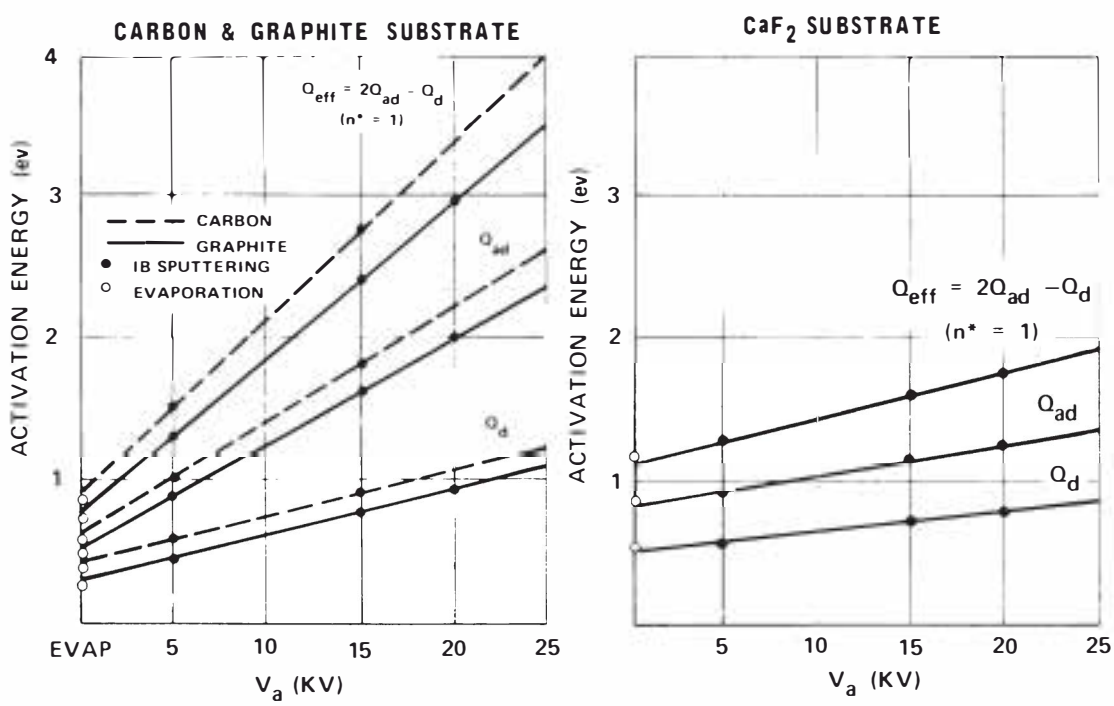

Fig. 17. IB voltage effect on activation energies.

© Kluwer Academic Publishers • Provided by the NASA Astrophysics Data System

1979Ap&SS..65..129K

(4) Independent of particle flux and kinetic energy, and substrate the binding energy Ge–Ge, which only applies to $n^* > 1$, i.e. single crystal condensation in this case, $E_{n^*} \cong 1.5$ eV.

The substrate effects indicated in the differences of Q_d and Q_{ad} are, of course, expected.

The kinetic energy effect is also clearly revealed as shown in Figure 17 for both the 'soft' and 'hard' substrates. In conformance with the embedding model, the effect on Q_{ad} is strongest on carbon and graphite, and has also a larger effect on Q_d on these substrates. The quantity Q_d stands for an 'effective activation' energy of diffusion and increases in both cases, but less than Q_{ad} due to combined embedding and surface mobility effects.

6. Structural Characteristics and Transition Condition of the Condensate

The results presented in the preceding sections have shown distinct differences in nucleation kinetics for each different structural phase of the condensate. Each phase could be associated with a sharply defined range of conditions, except for the glassy to crystalline transition which, in addition, was time dependent. Figure 18 schematically illustrates the observations by electron diffraction and micrography of the structural phases observed in various stages of condensation. While the data are for depositions on CaF_2, they are typical for all experiments. Five distinct phases are identified. Starting at the bottom, i.e. with the lowest temperatures, all deposits are glassy or amorphous from early nucleation through the formation of a continuous film. In a slightly higher temperature range, the time dependent amorphous to crystalline transition discussed previously results in purely polycrystalline films when the process is complete. The recrystallization process is indicated by formation of crystallites from surrounding amorphous growth as is evidenced by depletion halos. An additional region of special interest exists at a higher temperature. Here the initial nucleation occurs in the form of randomly oriented crystalline cluster, which in time are reoriented and ordered to form a single crystal condensate. In intermediate stages both random and preferentially oriented crystallites can be observed. Finally, in the highest temperature regions, only preferentially oriented crystallites are observed from the very initial nucleation stages through continuous film formation. The three schematics on top of each column show the general trend of the conditions leading to glassy, polycrystalline (random orientation) and single crystalline (preferred orientation) condensation as well as the typically well-defined transition conditions. The important feature is that the transitions for the very initial deposits do not coincide with those in the final state of continuous film formation. However, the four transitions occurring in the intermediate condensation stages coincide with the initial and final transitions respectively.

© Kluwer Academic Publishers • Provided by the NASA Astrophysics Data System

1979Ap&SS..65..129K

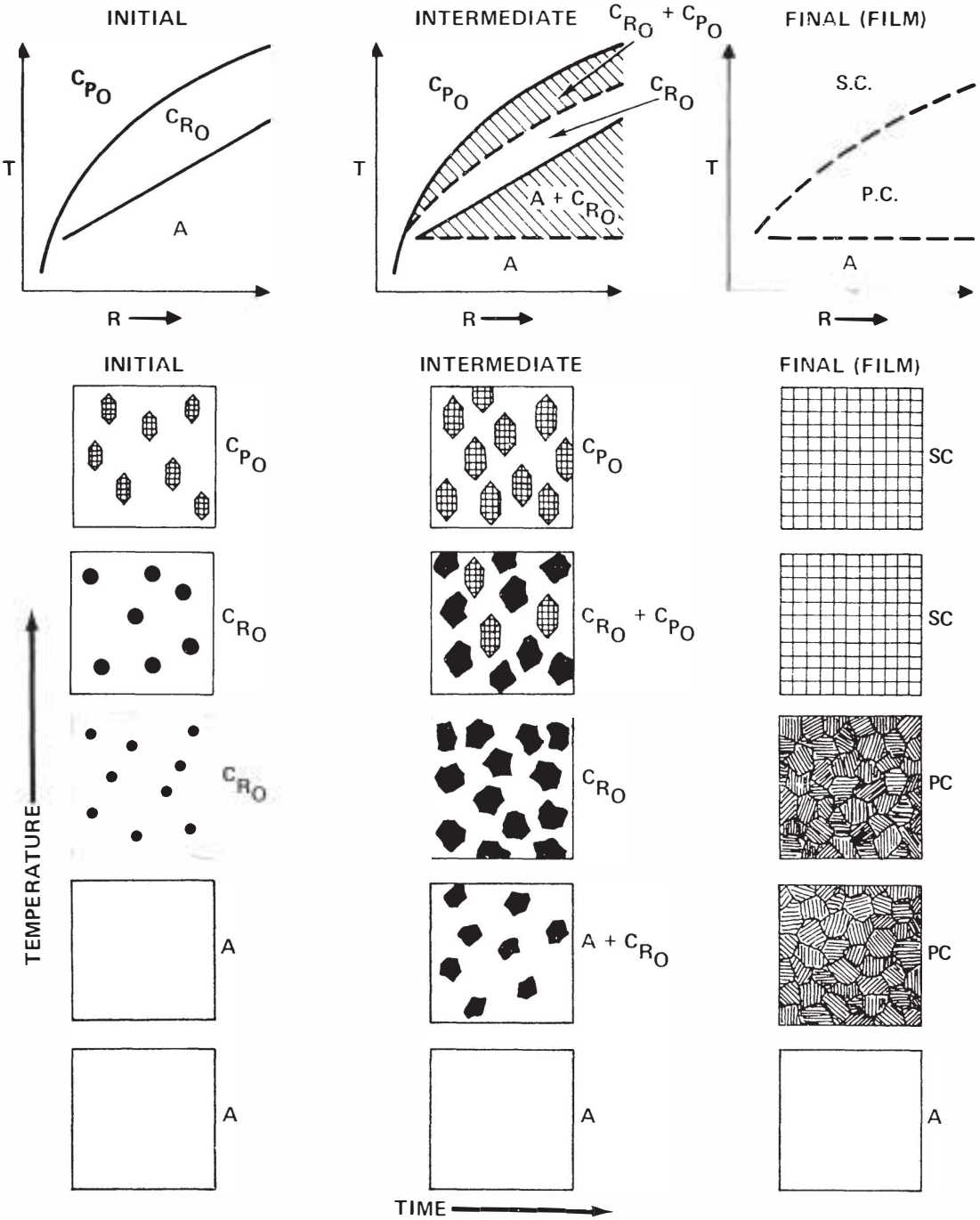

Fig. 18. Upper portion – transition conditions. Lower portion – actual film formation stages. A, Amorphous; C_{RO}, randomly oriented crystallites; C_{PO}, preferentially oriented crystallites; PC, polycrystalline, SC, single crystalline.

Figure 19 shows the same transformation schematic. However, additional temperature and time intervals are introduced to illustrate, for the lower order phases, the trends of $\bar{n}$ and $\bar{D}$ with time and temperatures. The density $\bar{n}$ increases with time as expected for all phases. However, in the crystalline region $\bar{n}$ decreases with temperature, as typical in a condensation process, but $\bar{n}$ increases with temperature in the

© Kluwer Academic Publishers • Provided by the NASA Astrophysics Data System

1979Ap&SS..65..129K

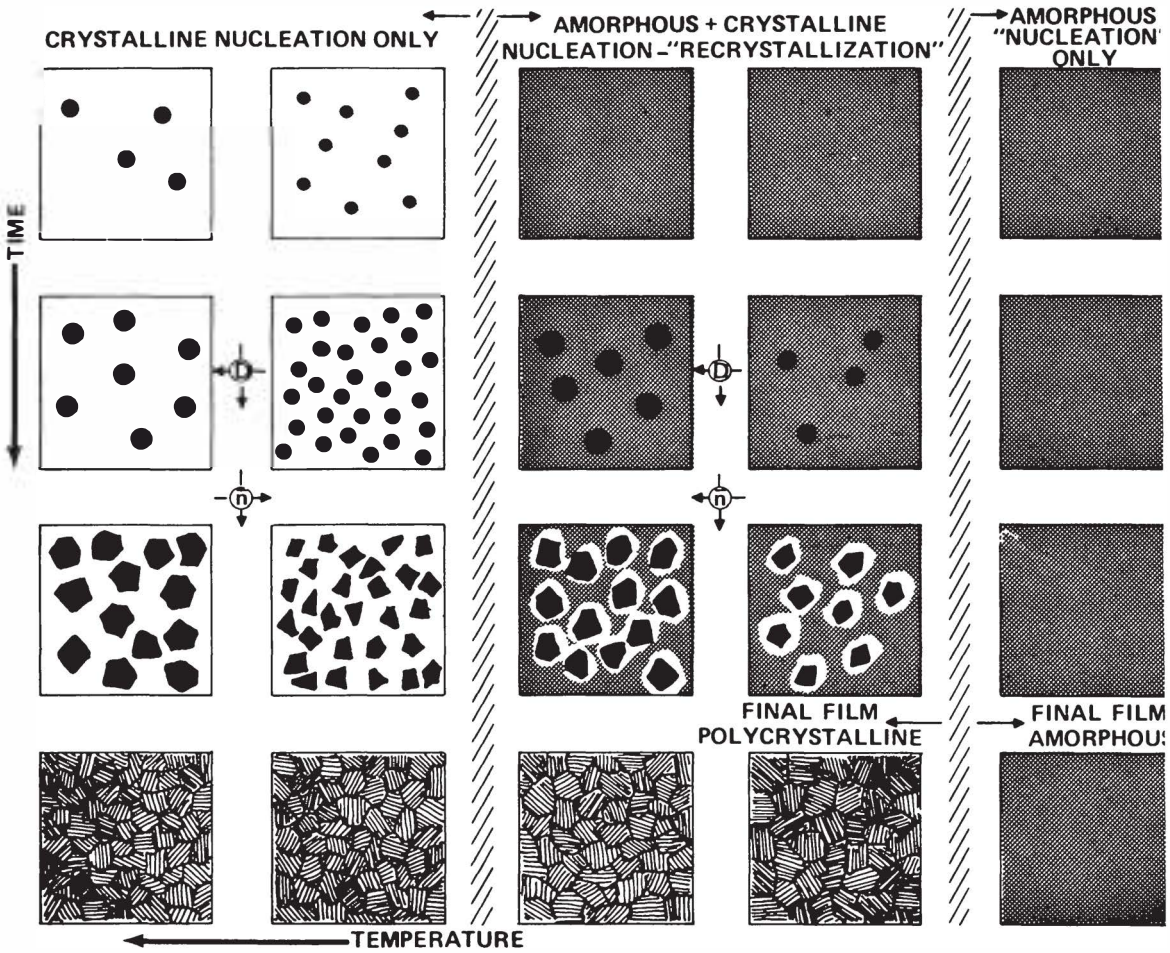

Fig. 19. Amorphous to crystalline transition.

regions of the time dependent amorphous to polycrystalline transition – i.e., in the recrystallization region. This conforms, of course, to the arguments and data presented in the discussion on condensation kinetics.

The schematics in Figures 18 and 19 served primarily in assisting the analysis of actual micrographs such as shown in Figures 20–23 with corresponding diffraction patterns. Figure 20 exemplifies the low temperature condensation behavior yielding amorphous deposits for all stages, while Figure 21 illustrates the amorphous to polycrystalline transition behavior at a higher temperature. Close inspection shows the formation of crystallites at the expense of the initial amorphous deposit. This is indicated by the light depletion region or halos. The formation of a final polycrystalline film is also apparent. Finally, Figures 22 and 23 give examples of high temperature behavior by showing a case where condensation proceeds totally polycrystalline (random orientation) and a case experiencing a polycrystalline to single crystalline transition as condensation progresses.

The desired end result of all these studies is illustrated in Figure 24 with actual results from one set of experiments, the nucleation and condensation of germanium

© Kluwer Academic Publishers • Provided by the NASA Astrophysics Data System

1979Ap&SS..65..129K

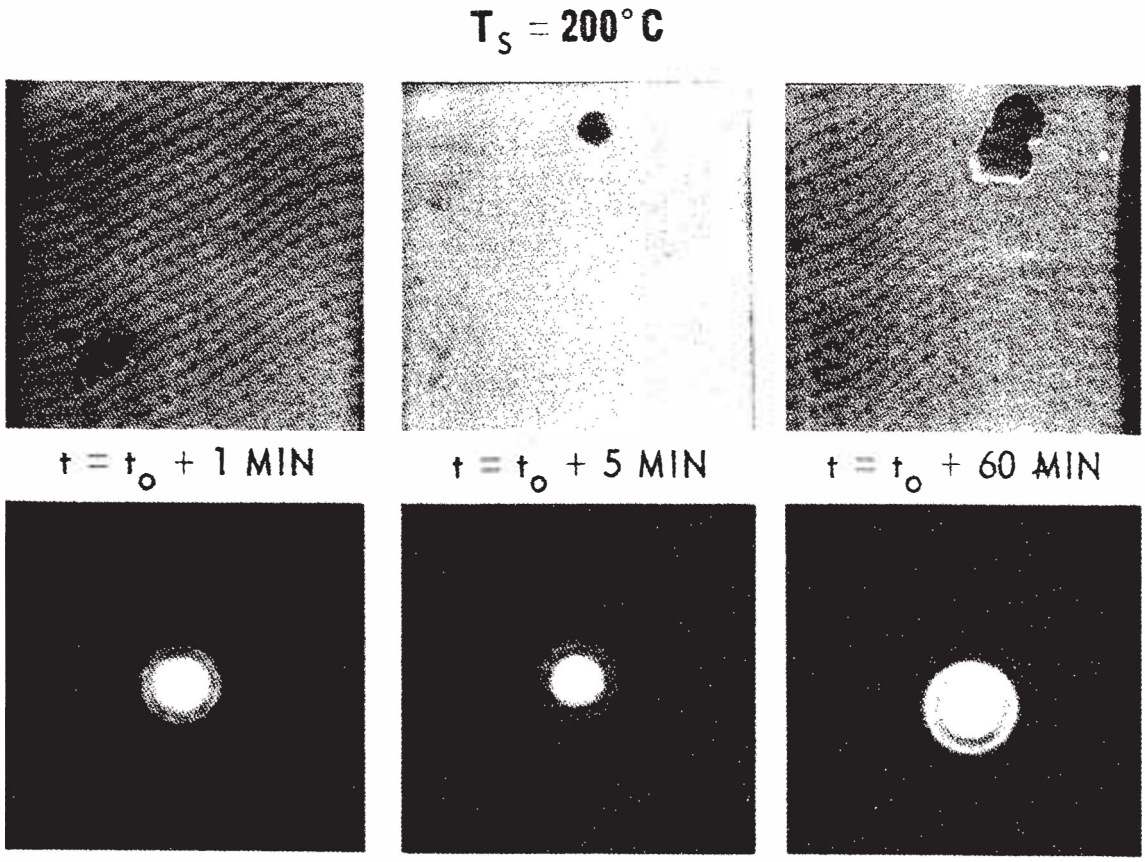

Fig. 20. Typical nucleation clusters (amorphous region) – Ge on carbon. 1 min, initial amorphous; 5 min, intermediate amorphous; 60 min, final film – amorphous.

on a CaF_2 substrate. The features are obviously those of the schematics in Figure 18. It shows the well defined regions, in which the appropriate combination of substrate temperature and growth rate produces amorphous, polycrystalline or single crystal condensation. As pointed out earlier, the growth rate is directly proportional to particle flux and was used only as a conveniently measurable parameter. Also, the nomenclature in C_{PO} and C_{RO} is used in early condensation phases, i.e. prior to cluster coalescence, to designate random and preferred orientations of crystalline nucleation clusters since the designations polycrystalline and single crystal are actually only meaningful in a continuous deposit.

The most interesting part of the structural phase diagrams are the well defined transition regions – usually repeatable to within a few degrees centigrade. Seen are the strong rate or flux dependencies of all crystalline transitions as well as the amorphous to crystalline transition in the early nucleation stage – i.e. when the process is entirely taking place by interaction between the adsorbates and the substrate. By contrast, the amorphous to crystalline transition at later stages occurs at one fixed temperature and is not flux dependent. This conforms to the model of recrystallization and the transition temperature corresponds to the recrystallization temperature of the germanium condensate. The crystalline transitions can quantitatively be expressed by

© Kluwer Academic Publishers • Provided by the NASA Astrophysics Data System

1979Ap&SS..65..129K

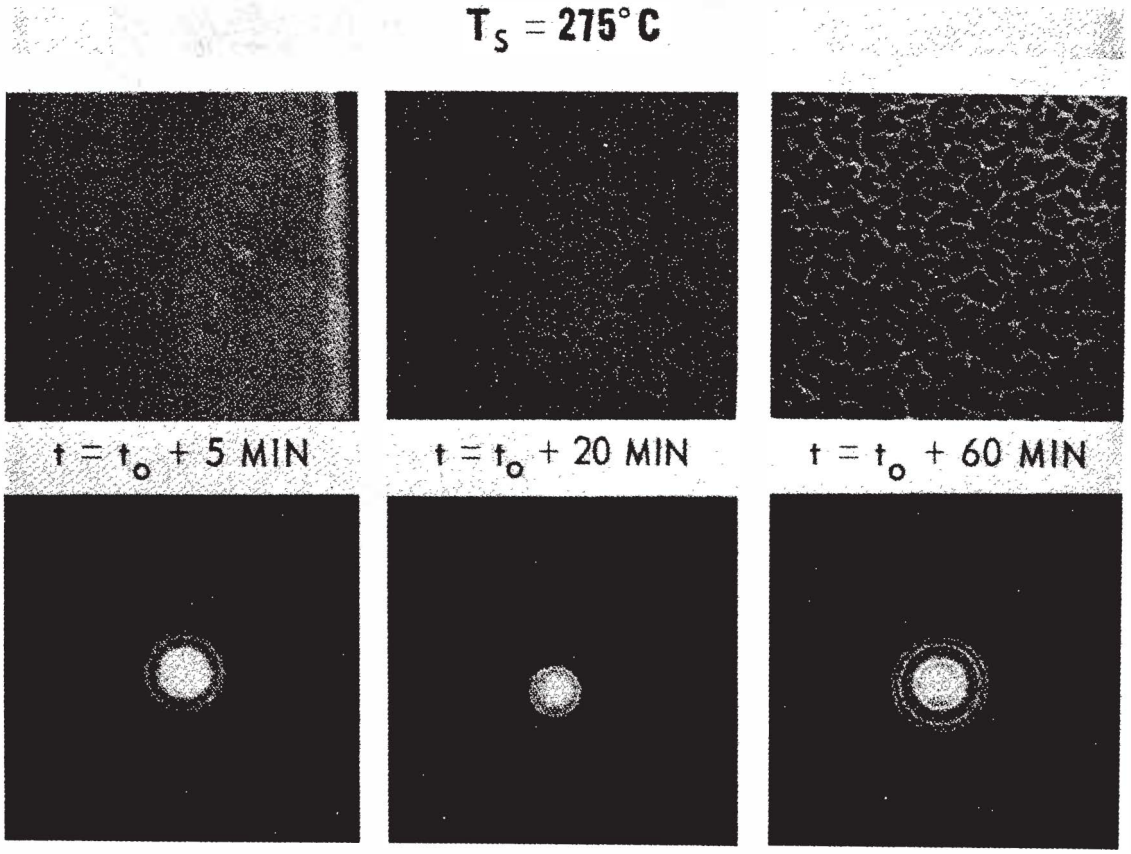

Fig. 21. Typical nucleation clusters – amorphous to polycrystalline transition (recrystallization region) – Ge on carbon. 5 min, initial amorphous; 20 min, intermediate amorphous plus crystallites; 60 min, final film – polycrystalline.

a rate equation with a well defined activation energy Q_{TR}. Reference is made here to Figures 14 and 16 where the activation energy is defined by $Q_{TR} = \frac{2}{3}(2Q_{ad} + E_2 - Q_d)$ which is essentially an equality of the activation energies describing the kinetics of the process for $n^* = 2$ and $n^* = 1$; i.e. for the nucleation of the poly- and single crystalline deposit, respectively. Obviously the original objective of the work was thus met. A full understanding and relatability of the initial nucleation behavior with the characteristics observed during thin film epitaxy (see Figure 1) was achieved.

As far as generality of these results are concerned, Figure 25 summarizes the various material systems investigated which exhibited behavior consistent with the data presented. As noted, monatomic systems as well as compound systems produced by reactive deposition and/or by direct deposition exhibit the same behavior.

In conclusion, we summarize in Figure 26 the observations achievable which make the reported approaches relevant to studies of condensation in a space environment. A significant fact is that all observations are controlled by characteristics of the particles formed in the vapor prior to adsorption. Examples are the effects of flux and particle kinetic energy. Also relevant to vapor effects are the results of a study (Krikorian and Sneed, 1966, 1967) on metal oxide condensation. The results of this study led to

© Kluwer Academic Publishers • Provided by the NASA Astrophysics Data System

1979Ap&SS..65..129K

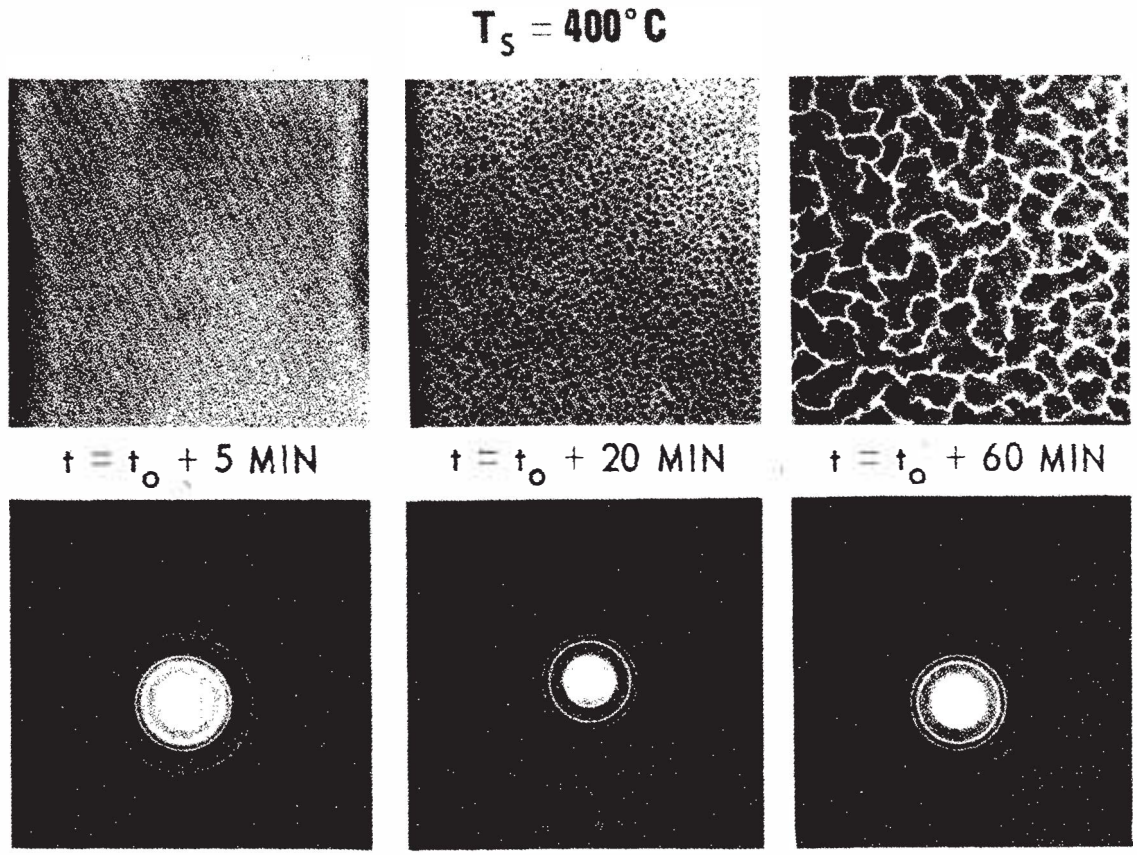

Fig. 22. Typical nucleation cluster (polycrystalline region) – Ge on carbon. 5 min, initial – polycrystalline; 20 min, intermediate – polycrystalline; 60 min, final film – polycrystalline.

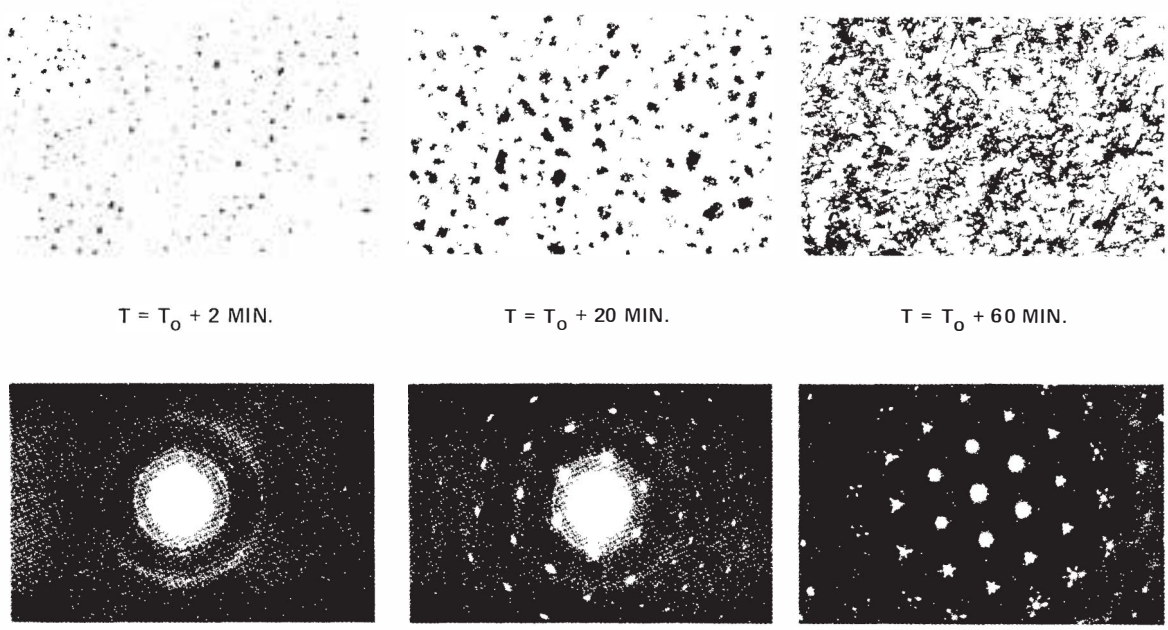

Fig. 23. Randomly oriented plus epitaxial cluster deposits – (reorientation region) – Ge on $CaF_2(111)$. 2 min, initial – random orientation; 20 min, intermediate random orientation + preferred orientation; 60 min, final film – single crystal.

© Kluwer Academic Publishers • Provided by the NASA Astrophysics Data System

1979Ap&SS..65..129K

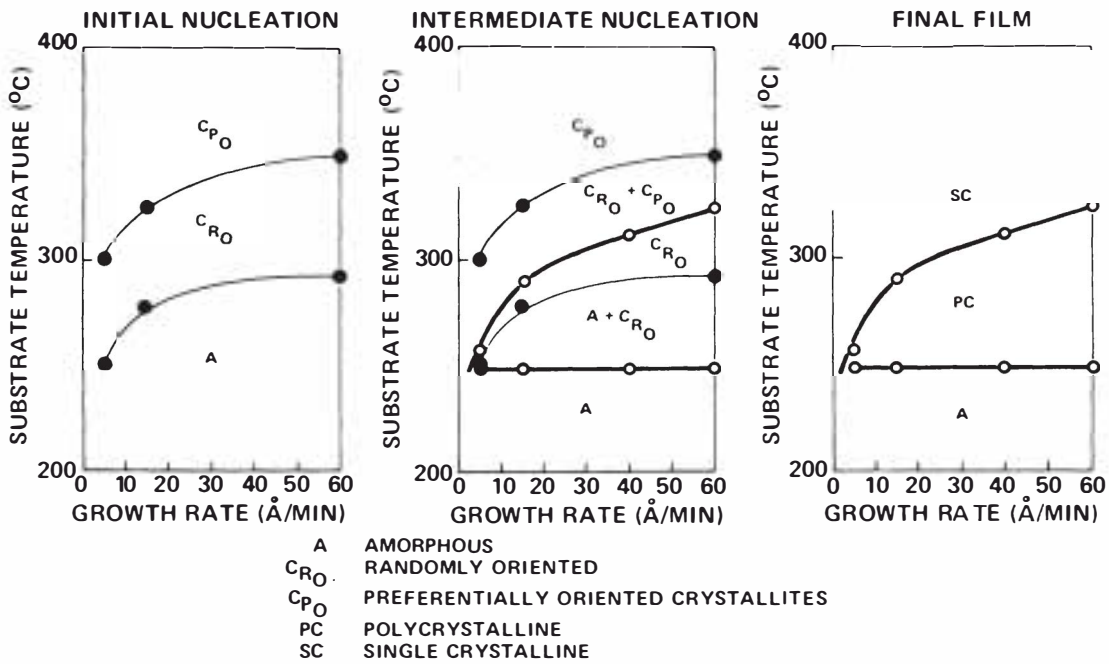

Fig. 24. Transition conditions during formation of Ge film on CaF_2 (UHV evaporation).

CONDENSATION BEHAVIOR – DIRECTLY STUDIED BY NUCLEATION EXPERIMENTS

Ge

Ta

Ag

CONDENSATION BEHAVIOR – DEDUCED FROM THIN FILM BEHAVIOR

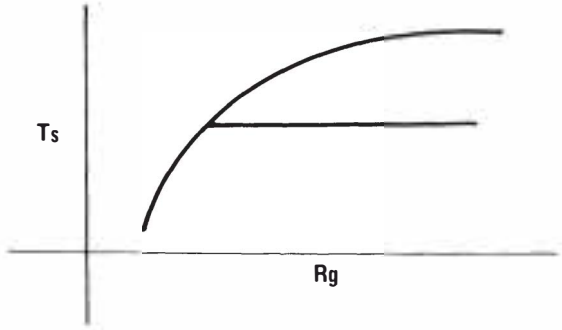

Ge	Ta_2O_5	(DIRECT AND REACTIVE)	ZnS
Ta	Al_2O_3	(DIRECT AND REACTIVE)	Ta1Y PbTe
Ag	C_eO		$Pb_{1-x}Sn_xT_e$ $Pb_{1-x}S_{nx}Se$ GaAs

Fig. 25. Generality of results. Material systems studied showing similar condensation behavior.

© Kluwer Academic Publishers • Provided by the NASA Astrophysics Data System

1979Ap&SS..65..129K

- DIRECT OBSERVATIONS
  - CRITICAL NUCLEUS SIZE, NUCLEATION DENSITY LIMITS AND GROWTH KINETICS
  - SUBSTRATE EFFECTS, EFFECTS OF ADSORBENT KINETIC ENERGY
  - CONDITIONS CONTROLLING STRUCTURE OF DEPOSITS AND STRUCTURAL TRANSFORMATIONS
- INDIRECT OBSERVATIONS
  - ANALYZE DEPOSIT ON SOLID SURFACES FOR DIFFERENCES IN:
    - ACTIVATION ENERGIES OF DIFFUSION AND ADSORPTION
    - ACTIVATION ENERGIES OF FILM GROWTH AND STRUCTURAL TRANSITIONS
    - COMPOSITION AND CELL STRUCTURE
    - FORMATION RATES OF NUCLEATION CLUSTERS
    - MANY OTHER CHARACTERISTICS YET TO BE DEFINED
  - ALL ARE CONTROLLED BY CHARACTERISTICS OF PARTICLES "FORMED" IN THE GASEOUS CLOUD PRIOR TO ADSORPTION

  (EXAMPLE: OXIDE FORMATION FROM METAL-OXYGEN VAPOR)

Fig. 26. Relevancy of presented material.

positive proof as to whether the oxide particles are formed on the substrate, i.e. after adsorption of metal atoms and oxygen atoms, or molecules, or in the metal oxygen vapor prior to deposition. The differences in activation energies of surface diffusion for metal, oxygen and oxides gave the clue. This study indicated that the methods used in this work for the study of condensation on solid surfaces can also be used for a study of condensation in a vapor or dust cloud.

References

Krikorian, E. and Sneed, R. J.: 1966, *J.A.P.* **37**, 3665.
Krikorian, E. and Sneed, R. J.: 1966, *J.A.P.* **37**, 3676.
Krikorian, E. and Sneed, R. J.: 1967, Technical Report AFAL-TR-67-139 August.

© Kluwer Academic Publishers • Provided by the NASA Astrophysics Data System